A High-Resolution Penalization Method for large Mach number Flows in the presence of Obstacles

Olivier Boiron, Guillaume Chiavassa, Rosa Donat

A High-Resolution Penalization Method for large Mach number Flows in the presence of obstacles

O. Boiron[a], G. Chiavassa[b], R. Donat[c]

[a]*Ecole Centrale Marseille and IRPHE UMR 6594, 13451 Marseille, France*
[b]*Ecole Centrale Marseille and M2P2 UMR 6181, 13451 Marseille, France*
[c]*Dept. Matematica Aplicada, Universidad de Valencia, Valencia, Spain*

Abstract

A penalization method is applied to model the interaction of large Mach number compressible flows with obstacles. A supplementary term is added to the compressible Navier-Stokes system, seeking to simulate the effect of the Brinkman-penalization technique used in incompressible flow simulations including obstacles. We present a computational study comparing numerical results obtained with this method to theoretical results and to simulations with Fluent software. Our work indicates that this technique can be very promising in applications to complex flows.

Key words: Brinkman Penalization, Complex geometries, Compressible Navier-Stokes Equations, Shock Waves.

1 Introduction

The treatment of complex geometries, and the associated boundary conditions, together with the presence of shocks, are two main difficulties in numerical simulations involving compressible flows in problems of practical engineering relevance such as flow over the wings and fuselage of rockets and airplanes. When considering the compressible Navier-Stokes equations to model high Mach flows, an adequate numerical treatment of shock waves can be achieved through the use of high-resolution shock capturing (HRSC) techniques in the

---

discretization of the convective fluxes. On the other hand, the presence of obstacles in the flow is a complex issue that has been handled using a variety of techniques, from coordinate transformations and body fitted structured and unstructured grids to fictitious domain approaches [13,19].

The body-fitted unstructured mesh approach in particular seems to have gained momentum within the shock capturing community, since it undoubtedly provides a highly effective means of simulating flows around geometrically complex bodies. However, as noted in [27], the tendency to use unstructured grids should be counterbalanced by various considerations. On one hand, there is nowadays a variety of high-resolution shock capturing schemes that are robust and reliable, and very easily implemented on Cartesian meshes. There is also numerical evidence that suggests that for very strong shocks, schemes which employ unstructured grids suffer from larger phase errors than do schemes which employ structured grids. Lastly, as pointed out in [27], given the increased reliance placed on computational results, different alternatives should be proposed, analyzed and compared in order to have different codes to cross-check numerical results.

Cartesian boundary methods provide an alternative to the unstructured approach (see e.g. [27,21,22,9] and references therein). Conceptually, the embedded boundary approach is quite simple: solid bodies blank out an area in a background cartesian mesh and the 'cut cells' receive special attention during the numerical integration of the flow solution. It is widely understood that the major obstacle faced by these schemes lies in formulating a general strategy for cut cells that can cope with truly complex geometries. Small cut cells often lead to accuracy losses and/or strict time step restrictions. These concerns have been addressed in the literature [27,22,12,9], but the resulting algorithms are still rather complex.

A different set of techniques stems from the penalization method introduced by E. Arquis and J.P. Caltagirone [3]. The physical idea of this penalization technique is to consider the obstacle as a porous media with porosity tending to zero. This corresponds to a Brinkman-type model, where the fluid domain has a large permeability in front of that of the porous medium.

The basic design of the method for incompressible flows, as described by Angot *et al.* in [2] is as follows: solid bodies are described by a mask function with value 1 inside the obstacle and 0 outside. The momentum equations in the Navier-Stokes system are modified by adding a supplementary term with the idea of forcing the velocity to satisfy the no-slip conditions ($(u, v) = (0, 0)$) on the body of the obstacle. The new system is then solved in an obstacle-free computational domain. Convergence theorems and rigorous error estimates when the penalization parameter tends to zero are established in [2].

From a practical point of view, the use of the the mask function implies that the incompressible Navier Stokes equations are being considered in the fluid domain, while there is a *fictitious fluid* within the solid body that evolves by

2

the full penalized system. Around the solid boundary, the computed values for the real fluid and the fictitious fluid influence each other.

Since the penalized system is solved in an obstacle-free domain, fast and effective methods for Cartesian grids can be used. Different numerical simulations of viscous flows using adaptive wavelet methods [31,17,34], pseudospectral methods [16], or finite difference/volume methods [2,18,26], have put in evidence the efficiency of this technique for incompressible flow simulations. The underlying numerical scheme provides the computational framework for the interplay between the real and the fictitious fluids. The complete algorithm becomes then a general strategy that can cope with complex geometries in a rather automatic manner.

The benefits of a similar penalization technique for compressible flows are evident, since it would allow the use of well established discretization techniques for compressible flows on regular Cartesian meshes. Driven by applications in computational aeroacoustics, and using an underlying adaptive wavelet collocation method [34] in the time marching procedure, Q. Liu and O. Vasiliev propose in [23] a penalization technique for the compressible Navier-Stokes equations and apply it to acoustic problems. A related penalization technique has been proposed also by Y. Cho, S. Boluriaan and P. Morris [5] for a $\kappa - \omega$ turbulence model for high Reynolds number simulations.

The Penalization technique proposed in [7] and analyzed in this paper is formally different from the two mentioned before. It successfully merges a HRSC discretization of the convective fluxes in the Navier-Stokes system with a particular form of the penalization term that allows for an efficient solution algorithm, whose global cost is considerably reduced by the use of the multilevel technique developed by Chiavassa and Donat in [6]. We should remark that the simulations in [23,5] only deal with low Mach number flow. On the other hand, preliminary results with the present algorithm (see [7]) show that the proposed penalization technique, together with a HRSC treatment of the convective fluxes in the Navier-Stokes system, leads to an accurate simulation of high Mach number shocked flows around obstacles of arbitrary shape.

To the best of our knowledge, there is no theoretical proof that the solution to the penalized system tends to the solution of the compressible Navier-Stokes equations when the penalization parameter goes to zero. Nevertheless, our computational study indicates that our penalization technique provides numerical results which are consistent with physical properties of the flows under consideration.

In this paper we examine several features of our penalization technique. Our numerical results indicate that the penalization parameter controls, as in the incompressible case, the effective application of Dirichlet boundary conditions on the solid body. In addition, we compare the results obtained from the simulations with our penalization technique to the results obtained with the all-purpose commercial Fluent code, obtaining a good agreement in global

3

and local behavior of the computed flows. Finally, these numerical results are compared with well known results from inviscid flow theory, when this comparison is relevant. For the considered high Mach and high Reynolds flows, the resulting flow should behave as an inviscid flow sufficiently far from the obstacle. As before, the numerical results are absolutely consistent with the theoretical inviscid values.

The paper is organized as follows. In section 2 the physical problem and the governing equations are given. The penalization method is described in section 3 and in section 4 we give specific details on the numerical technique we use in the simulations. The results of various numerical simulations are shown in section 5. Finally, we draw some conclusions in section 6.

2   Physical setting: Geometry and governing equations

Let Ω be a regular open set in $I\!\!R^2$ (the computational domain) containing N fixed regular obstacles Ω_s^n, $1 \leq n \leq N$. We set

$$\Omega_s = \bigcup_{n=1}^{N} \Omega_s^n, \qquad \Omega_f = \Omega \backslash \overline{\Omega}_s,$$

so that $\overline{\Omega}_s$ is the (closed) region occupied by the solid bodies and Ω_f is the fluid domain.

The flow around the obstacles Ω_s is modeled by considering the full compressible Navier-Stokes equations on the fluid domain, together with appropriate boundary conditions on the boundary of the solid bodies $\Gamma_s^n = \partial \Omega_s^n$. Appropriate inflow/outflow boundary conditions have to be provided also, for computational reasons, on the outer boundary of Ω, Γ. Hence, we shall consider initial boundary-value problems (IBVP) as follows,

$$\begin{cases} \partial_t \overrightarrow{U} + \nabla \overrightarrow{F}(\overrightarrow{U}) = \dfrac{1}{Re} \nabla \overrightarrow{F_V}(\overrightarrow{U}), & (X,t) \in \Omega_f \times I\!\!R^+, \\[2mm] \overrightarrow{U}(X, t=0) = \overrightarrow{U_0}(X) & \text{in } \Omega_f, \\[2mm] \text{boundary conditions} & \text{on } \Gamma \text{ and } \Gamma_s^n. \end{cases} \quad (1)$$

As usual, $\overrightarrow{U} = (\rho, \rho u, \rho v, E)^T$ is the vector of dimensionless conservative variables, ρ being the density of the fluid, u and v the components of fluid velocity, and E the total fluid energy. The Reynolds number is defined through a reference velocity u_0, density ρ_0, length l_0 and viscosity μ_0 by $Re = \frac{\rho_0 l_0 u_0}{\mu_0}$.

The convective flux vector $\overrightarrow{F} = (f(\overrightarrow{U}), g(\overrightarrow{U}))$ is classically defined as

$$f(\overrightarrow{U}) = (\rho u, \rho u^2 + p, \rho uv, (E+p)u)^T$$

$$g(\overrightarrow{U}) = (\rho v, \rho uv, \rho v^2 + p, (E+p)v)^T, \tag{2}$$

while the viscous flux-vector $\overrightarrow{F_V} = (f_V(\overrightarrow{U}), g_V(\overrightarrow{U}))$ is defined by

$$f_V(\overrightarrow{U}) = \left(0, \tau_{xx}, \tau_{xy}, u\tau_{xx} + v\tau_{xy} + \frac{\gamma}{Pr}e_x\right)^T$$
$$g_V(\overrightarrow{U}) = \left(0, \tau_{yx}, \tau_{yy}, u\tau_{yx} + v\tau_{yy} + \frac{\gamma}{Pr}e_y\right)^T \tag{3}$$

where τ is the stress tensor, with the usual definitions corresponding to a Newtonian fluid (see e.g. [1] for specific details), $\gamma = \frac{c_p}{c_v}$ is the constant specific heat ratio and Pr is the Prandtl number.

System (1) is closed by the equation of state for a polytropic gas:

$$p = (\gamma - 1)\rho e, \tag{4}$$

where e stands for the internal fluid energy, linked to the temperature T and to the total energy E by the relations

$$e = c_v T, \quad E = \rho e + \frac{1}{2}\rho(u^2 + v^2). \tag{5}$$

On the surface of each solid obstacle, Ω_s^n, the fluid velocity must satisfy the no-slip condition,

$$u_{|\Gamma_s^n} = v_{|\Gamma_s^n} = 0. \tag{6}$$

We shall only consider Dirichlet boundary conditions for the temperature, that is, we assume that the wall temperature on each obstacle is fixed to a given value $T_{\Omega_s^n}$, i.e

$$T_{|\Gamma_s^n} = T_{\Omega_s^n}. \tag{7}$$

The necessary outflow or inflow boundary conditions, imposed at the outer boundaries of Ω depend of the problem, and shall be described in section 5.

3 The penalization method

The basic idea underlying all penalization techniques for incompressible flow proposed in the literature is to enforce the no-slip boundary conditions by adding a penalized velocity term in the momentum equation. In [3,2], the penalization term

$$\frac{1}{\eta} \chi_{\Omega_s} \begin{pmatrix} u \\ v \end{pmatrix}, \tag{8}$$

where χ_{Ω_s} is the characteristic (or mask) function of the solid domain Ω_s, is added to the momentum equation of the incompressible Navier-Stokes system. This technique corresponds to a Brinkman-type porous media model with variable permeability, where the fluid domain has a very large permeability in front of that of the obstacle, and it has been applied successfully in many configurations (fixed and moving obstacles) [2,16,18,31,17,34].

The analysis carried out in [2] demonstrates that the solution of the penalized system converges to the solution of the incompressible Navier-Stokes system in the fluid domain, and that the velocity converges to zero in the solid domain at a theoretical rate of $O(\eta^{3/4})$. This demonstrates that the penalization parameter provides an effective tool in order to enforce the no-slip boundary condition at the boundary of a solid body in incompressible flow. It is worth mentioning that an effective convergence rate of $O(\eta)$ for the velocity field inside the obstacle has been found in all numerical experiments, instead of the theoretical estimate of $O(\eta^{3/4})$ proven in [2].

For compressible Navier-Stokes flow, the boundary condition includes also the temperature (7), so that penalized terms need to be included both in the equations for conservation of momentum and energy. In [23], penalized terms including the velocity and the temperature are added to the momentum and energy equations. In addition, the continuity equation for porous media is considered inside the obstacle to make the model compatible with compressible flow through porous media.

The penalization technique proposed in [7] considers instead penalization terms that involve directly the momentum and the global energy as follows

$$
\begin{cases}
\partial_t \overrightarrow{U_\eta} + \nabla \overrightarrow{F}(\overrightarrow{U_\eta}) + \frac{1}{\eta} \chi_{\Omega_s} \begin{pmatrix} 0 \\ \rho_\eta u_\eta \\ \rho_\eta v_\eta \\ E_\eta - E_{\Omega_s} \end{pmatrix} = \frac{1}{Re} \nabla \overrightarrow{F_V}(\overrightarrow{U_\eta}), \ (X,t) \in \Omega \times \mathbb{R}^+, \\
\overrightarrow{U_\eta}(X, t = 0) = \overrightarrow{U_0}(X) \ \text{ in } \Omega, \\
+ \text{ boundary conditions on } \Gamma,
\end{cases}
\tag{9}
$$

where $\overrightarrow{U_\eta}$ represents the vector of unknowns, depending now on the parameter η (η is small $0 < \eta \ll 1$), and E_{Ω_s} is the 'energy' of the solid body Ω_s, whose value is given in terms of the fixed wall Temperature T_{Ω_s} by

$$
E_{\Omega_s} = \rho_\eta c_{\mathrm{v}} T_{\Omega_s}.
\tag{10}
$$

The expression of the penalization terms above is inspired also by efficiency requirements in applying the multilevel-HRSC technology in order to be able to compute accurate simulations of high Mach number flows. We observe that including directly the momentum in the penalization term, instead of the ve-

locity as in the incompressible case, makes it possible to solve efficiently the system derived from an implicit treatment of the penalization terms. The following derivation shows that the penalization term for the energy equation effectively enforces a Dirichlet condition on the temperature, while maintaining the aforementioned efficiency.

A formal asymptotic analysis, as performed in [2], can be readily carried out by writing formally

$$\begin{cases} \rho_\eta = \rho + \eta\tilde{\rho}, \ u_\eta = u + \eta\tilde{u} \\ e_\eta = e + \eta\tilde{e} \ v_\eta, = v + \eta\tilde{v} \end{cases} \tag{11}$$

from which we easily deduce that $E_\eta = E + \eta\tilde{E}$, $T_\eta = T + \eta\tilde{T}$ and $p_\eta = p + \eta\tilde{p}$ where the $O(1)$ variables ρ, e, u, v, E, p, T are related by the usual relations (4) and (5). Let us introduce these variables into system (9) and denote $\overrightarrow{U} = (\rho, \rho u, \rho v, E)^T$. Then, one easily gets by identifying the terms of order η^{-1}:

$$\chi_{\Omega_s} \left(0, \rho u, \rho v, E - \rho c_{\mathrm{v}} T_{\Omega_s}\right)^T = 0, \tag{12}$$

while for the order η^0 terms we obtain:

$$\partial_t \overrightarrow{U} + \nabla \overrightarrow{F}(\overrightarrow{U}) + \chi_{\Omega_s} \begin{pmatrix} 0 \\ \rho\tilde{u} + \tilde{\rho}u \\ \rho\tilde{v} + \tilde{\rho}v \\ \tilde{E} - \tilde{\rho}c_{\mathrm{v}}T_{\Omega_s} \end{pmatrix} = \frac{1}{Re}\nabla\overrightarrow{F}_V(\overrightarrow{U}). \tag{13}$$

In the fluid domain ($X \in \Omega_f$), the mask function χ_{Ω_s} is zero and (13) reduces to the initial Navier-Stokes system (1). Hence, as in [2], we formally have that $\overrightarrow{U}$ is a solution of the compressible N-S equations on the fluid domain.

Inside of the obstacle $\chi_{\Omega_s}(X) \equiv 1$, hence relation (12) reduces to

$$\rho u = \rho v = 0 \quad \text{and} \quad E = \rho c_{\mathrm{v}} T_{\Omega_s}, \qquad X \in \Omega_s. \tag{14}$$

Because of the above, the first equation in system (13) becomes inside the obstacle

$$\partial_t \rho = 0, \text{ in } \Omega_s. \tag{15}$$

Thus, the density remains constant in the solid, and it follows from (14) that $u = v = 0$ in the obstacle, i.e. the velocity field satisfies the no-slip boundary condition. In addition, from equation (5) for the global energy, we readily get that $E = \rho c_{\mathrm{v}} T$ in Ω_s, hence we recover, thanks to (14), the temperature boundary condition (7).

This formal analysis, which proceeds as in the incompressible case, intends to show that the vector $\overrightarrow{U}$ defined by relations (11) verifies the Navier-Stokes equations in the fluid domain and the correct boundary conditions on the obstacles. Since there is no analytical proof of the convergence of the penalized solution $\overrightarrow{U}_{\eta}$ to $\overrightarrow{U}$, the solution of the Navier-Stokes system (1), we shall carry out a series of numerical experiments in section 5 in order to examine whether the flow obtained from the penalized system (9) is physically correct. The numerical results of section 5 seem to indicate that this penalization method can be used efficiently for the simulation of shocked flows with obstacles. The robustness of the numerical treatment of the convective terms (see section 4) allows us to obtain high resolution simulations for high Mach number flows.

Remark Taking into account that $u = v = 0$ in Ω_s, the second and third equations in (13) become

$$\nabla p + \rho(\tilde{u}, \tilde{v})^T = 0, \quad X \in \Omega_s. \tag{16}$$

Thus, since the density is constant, the gradient of the pressure is proportional to the velocity inside the obstacle, i.e. there is a Darcy law for the pressure inside the obstacle.

Remark From relations (12)-(16), it is possible, as in the incompressible case, to recover the force acting on the solid Ω_s by simply integrating the momentum equation over the volume of the obstacle:

$$\mathbf{F}_{\Omega_s} = \frac{1}{\eta} \int_{\Omega_s} \rho(u_{\eta}, v_{\eta})^T dX. \tag{17}$$

This property is particularly interesting from a computational point of vue, since the drag and lift can be computed very efficiently by a convenient approximation of the volume integral above, instead of a surface integral (see formula (30)).

In addition to the incompressible Navier-Stokes system, similar penalization techniques have been devised for the heat equation [16] and wave equation [26]. In both cases, a theoretical proof of the convergence of the solutions of the penalized system to the solution of the original system has also been obtained.

4   Numerical algorithm

We shall describe in this section the way we discretize and solve numerically the penalized system (9). Since the equations are now written in an obstacle

free domain Ω, we consider a Cartesian grid $\mathcal{G} = \{(x_i, y_j),\ 0 \le i \le N_x,\ 0 \le j \le N_y\}$ with uniform step sizes $\delta x, \delta y$, fully covering Ω.

In what follows, we omit the subscript η in the variables for simplicity reasons. Thus, $\overrightarrow{U}_{ij}$ will denote the approximation of $\overrightarrow{U}_\eta(x_i, y_j)$.

We discretize system (9) by a *method of lines*, which leads to the following system of ODEs at each point in the computational mesh:

$$\frac{d\overrightarrow{U}_{ij}}{dt} + D(\overrightarrow{U}_{ij}) + K(\overrightarrow{U}_{ij}) + H(\overrightarrow{U}_{ij}) = 0. \tag{18}$$

Here $D(\overrightarrow{U}_{ij})$ is the numerical divergence associated to the convective fluxes (see section 4.1), $K(\overrightarrow{U}_{ij})$ the finite difference approximation of the viscous fluxes (see section 4.2) and $H(\overrightarrow{U}_{ij})$ the approximation of the penalization term (see section 4.3). The system of ODEs (18) will be solved by a Runge-Kutta time integrator described in section 4.4.

4.1 Discretization of the inviscid fluxes

Since shocks are correctly and accurately computed by using the high resolution shock-capturing (HRSC) technology, we consider an approximation in *conservation form* for $D(\overrightarrow{U}_{ij})$ as follows

$$D(\overrightarrow{U}_{ij}) = \frac{\overrightarrow{F}_{i+1/2,j} - \overrightarrow{F}_{i-1/2,j}}{\delta x} + \frac{\overrightarrow{G}_{i,j+1/2} - \overrightarrow{G}_{i,j-1/2}}{\delta y}, \tag{19}$$

where $\overrightarrow{F}_{i+1/2,j} = \overrightarrow{F}\left(\overrightarrow{U}_{i-k,j}, \cdots, \overrightarrow{U}_{i+m,j}\right)$, $\overrightarrow{G}_{i,j+1/2} = \overrightarrow{G}\left(\overrightarrow{U}_{i,j-k}, \cdots, \overrightarrow{U}_{i,j+m}\right)$, with $\overrightarrow{F}$ and $\overrightarrow{G}$ HRSC numerical flux functions, consistent with the physical inviscid flux functions (2).

HRSC schemes of the ENO-WENO family in particular [30] are used routinely nowadays in compressible flow simulations involving inviscid Euler flows due to their robust behavior (see e.g. [6,28] and references therein). These schemes require the use of Cartesian grids, where they are both simple to implement and very efficient. Here, as in previous papers [6,28], we use a robust third order ENO-type scheme [10][24] to compute the numerical flux functions.

The multilevel cost-reduction strategy developed in [6] is also employed in order to reduce the computational cost associated to the HRSC computation of the numerical divergence. It follows an original idea of A. Harten [14] and is based on the fact that highly sophisticated shock-capturing numerical flux functions are only needed in the neighborhood of an existing discontinuity or in regions where singularities develop. In [6], a straightforward interpolating wavelet transform is used in order to analyze the regularity of the numerical

9

solution. The results in [6,28] show that, combined with the robust HRSC scheme of [10], the multilevel technique is capable to obtain the high quality expected of a HRSC scheme with a significant reduction in the global computational effort, hence in the CPU time of the simulation (for details and results see [6,28]).

The ideas of A. Harten in [14] have been extended by other authors in the framework of finite volume schemes for shock computations. We mention, for example, [8,29], where it is shown that computational savings in memory requirements can also be obtained by incorporating adequate data structures in the numerical code. This strategy can turn a wavelet-based adaptive scheme into a true adaptive mesh-refinement code (see [25]).

In the present paper, the multilevel technique reduces the effective CPU time associated to the computation of the numerical divergence (which is the main time consuming part of the full algorithm) by an average factor of 5.5 for uniform grids with 1536^2 points, of 4 for 1024^2, and of 3 for 512^2 grid points.

4.2 Discretization of the viscous fluxes

As usual, the viscous fluxes are discretized with a centered scheme. To be consistent with the order of the approximation of the convective term, we use fourth order accurate centered finite difference discretizations of the space derivatives involved in the viscous terms . The formulas for the first space derivatives are [15]:

$$
\begin{aligned}
(u_x)_{ij} &= \frac{u_{i-2,j} - 8u_{i-1,j} + 8u_{i+1,j} - u_{i+2,j}}{12\delta x} + \mathcal{O}(\delta x^4), \\
(u_y)_{ij} &= \frac{u_{i,j-2} - 8u_{i,j-1} + 8u_{i,j+1} - u_{i,j+2}}{12\delta y} + \mathcal{O}(\delta y^4),
\end{aligned}
\tag{20}
$$

and straightforward, but lengthy, algebra gives $K(\overrightarrow{U}_{ij})$ the space approximation of the viscous part of (9).

4.3 Discretization of the penalization term

Once the parameter η is fixed, the penalization term is treated as a source term and computed at each grid point $(x_i, y_j) \in \mathcal{G}$ by

$$
\begin{cases}
H(\overrightarrow{U_{ij}}) = 0 & \text{if } (x_i, y_j) \in \Omega_f, \\[2em]
H(\overrightarrow{U_{ij}}) = \frac{1}{\eta} \begin{pmatrix} 0 \\ (\rho u)_{ij} \\ (\rho v)_{ij} \\ (E - E_{\Omega_s})_{ij} \end{pmatrix} & \text{if } (x_i, y_j) \in \overline{\Omega}_s.
\end{cases}
\tag{21}
$$

This term requires only the knowledge of the geometry of the solid domain and adds no extra computation. This should be compared to the computational efforts needed by an adaptation of the grid around the obstacle or by a coordinate transformation.

4.4 The time discretization

The time integration of system (18) is carried out by using a third order TVD Runge-Kutta scheme described in [30], where the convective and viscous spatial terms are treated in an explicit fashion, while the penalization term is treated implicitly. Let

$$
L(\overrightarrow{U_{ij}}) = D(\overrightarrow{U_{ij}}) + K(\overrightarrow{U_{ij}}).
\tag{22}
$$

We consider the following three steps time integrator for equation (18):

$$
\begin{aligned}
\overrightarrow{U}^* &= \overrightarrow{U}^n - \delta t\, L(\overrightarrow{U}^n) - \delta t\, H(\overrightarrow{U}^*), \\
\overrightarrow{U}^{**} &= \tfrac{1}{4}\Big(3\overrightarrow{U}^n + \overrightarrow{U}^* - \delta t\, L(\overrightarrow{U}^*) - \delta t\, H(\overrightarrow{U}^{**})\Big), \\
\overrightarrow{U}^{n+1} &= \tfrac{1}{3}\Big(\overrightarrow{U}^n + 2\overrightarrow{U}^{**} - 2\delta t\, L(\overrightarrow{U}^{**}) - 2\delta t\, H(\overrightarrow{U}^{n+1})\Big).
\end{aligned}
\tag{23}
$$

The time step restriction due to stability for this scheme is $\delta t = \min(\delta t_e, \delta t_v)$, with δt_e the inviscid time step restriction,

$$
\delta t_e = C_1 \frac{\min(\delta x, \delta y)}{S^n_{max}},
\tag{24}
$$

where S^n_{max} is the maximum wave speed throughout the domain at the time level n, and δt_v the viscous time step defined as [15]:

$$\delta t_v = C_2 \Big(\min(\delta x, \delta y) \Big)^2 Re \frac{Pr}{\gamma \mu}. \qquad (25)$$

Notice that, since we are interested in simulations of supersonic flows at large Reynolds numbers, there is no need to treat the viscous terms implicitly. On the other hand, an explicit discretization of the penalization term $H(\overrightarrow{U}_{ij})$ would lead to a stability restriction of the form $\delta t \sim \eta$, which is untractable for the value of η considered in practical simulations (see section 5). The implicit treatment of the penalization terms requires the solution of a linear system at each time step. However, the specific form of $H(\cdot)$ makes this a diagonal system, hence *no extra work* is involved in practice, in comparison with a fully explicit scheme.

For the simulations we use $C_1 = 0.8$ and $C_2 = 0.5$. The time step is adapted automatically during the computation.

The penalized system has to be solved also in the solid domain, which, in principle, increases the computational time. However, except for a thin layer around the solid body boundary, the flow is constant inside of the solid (see sections 3 and 5), therefore the combination with the multilevel technique allows for a considerable reduction of the associated computational expense.

Notice that when the point $(x_i, y_j) \in \Omega_f$ the discrete function $H(\cdot)$ is zero, and we recover the classical third order TVD Runge-Kutta scheme. On the other hand, the scheme is only first order in time in the obstacle (i.e. when $H(\cdot)$ is non zero). This will be improved in the future by the use of a real third order semi-implicit Runge-Kutta scheme [35]. Our experience, however, indicates that the influence of this loss of accuracy does not affect significantly the overall resolution of the flow structure (see section 5).

5 Numerical results

We design a series of numerical experiments in order to determine whether or not the penalization technique is able to reproduce correct physical behavior for large Mach number flows.

In all the numerical experiments of this section, the computational domain Ω is prescribed to be a square ($0 \leq x \leq 2, 0 \leq y \leq 2$). Inlet flow quantities are fixed at $x = 0$ while non-reflecting boundary conditions (outflow) are prescribed at the other boundaries using zero-order extrapolation at ghost cells [20]. The dimensionless penalized Navier Stokes equations (9) are solved, with the

Reynolds number fixed to $Re = 5 \cdot 10^4$ and the Prandtl number to 0.72 for all the simulations. Only Dirichlet boundary conditions will be considered in this paper, hence, taking into account the results of our formal asymptotic analysis, we set initially the velocity $(u, v)|_{\overline{\Omega}_s} = (0, 0)$ and the temperature to the given boundary value T_{Ω_s}.

In section 5.1, we focus on numerical simulations of a shock-cylinder interaction in order to examine the influence of the penalization parameter η on the numerical results obtained with the penalization technique. In sections 5.2 and 5.3, we carry out simulations of supersonic flows around triangular and cylindrical bodies by marching to steady state with the equations in (9). The large value of the Reynolds number considered allows us to compare the numerical results to well known theoretical properties of inviscid flow theory, away from the obstacles. We do not focus in this paper on the behavior of boundary layers or vortex sheets.

Our results are also compared to the numerical simulations obtained with Fluent, a standard commercial code for CFD computations that uses a body-fitted unstructured grid. The density-based solver of Fluent was selected for solving the full Navier-Stokes equations (1), together with the no-slip boundary condition and Dirichlet temperature condition on the boundary of the solid obstacle. In the Fluent package [11], we selected second order accuracy for temporal and spatial (upwind schemes) accuracy. To ensure that the positions of the shock and expansion waves are appropriately resolved, the grid is dynamically refined during the calculation.

5.1 Unsteady flow: Influence of the penalization parameter

The first set of results intends to show that the formal asymptotic analysis shown in section 3 does indeed hold. In particular, we shall see that the density remains constant inside the obstacle, and that the penalized terms drive the velocity down to zero inside the obstacle, hence effectively enforcing the no-slip condition at the boundary, and the temperature to its specified value on the boundary of the obstacle.

We shall consider a shock-cylinder interaction, with initial configuration as described in figure 1: A Mach-3 shock wave ($M_s = 3$), initially located at $x = 0.1$, travels from left to right to interact with a solid circle of radius $r = 0.2$, centered at $(0.5; 1)$. In the flow domain Ω_f, the state variables at the right of the shock at time $t = 0$ are $(\rho_0, p_0, u_0, v_0) = (1, 1, 0, 0)$ and quantities at the left of the shock are computed from the ones at the right side and the Mach number M_s using classical shock considerations [33]. Inside the obstacle, i.e. in Ω_s, $\rho = 1$, and $T_{\Omega_s} = 3$. Energy and pressure are computed from relations
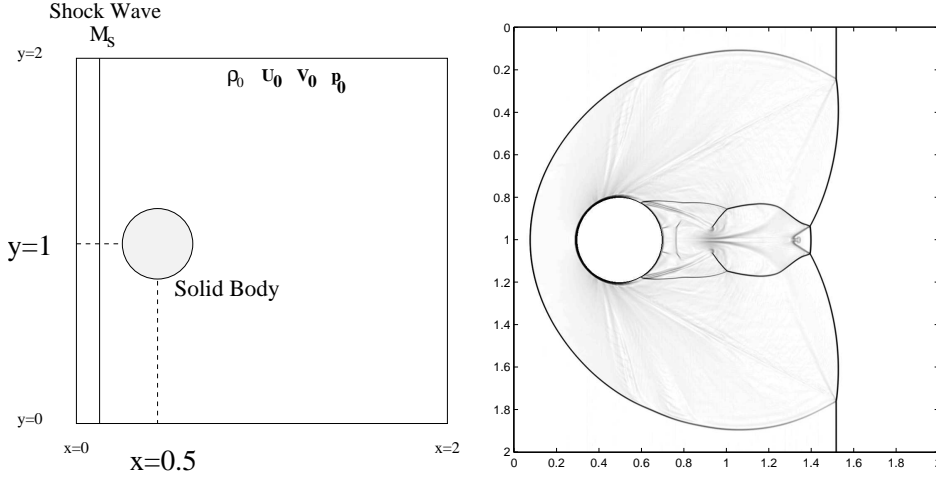
13

(4) and (5).

Fig. 1. Left: computational domain Ω and initial conditions for the shock-cylinder interaction of section 5.1. Right: Shock-cylinder interaction for $M_s = 3$. Numerical Schlieren image obtained from the density at time $t = 0.4$ for 1024^2 grid points and penalization parameter $\eta = 10^{-12}$.

To address the issue of the influence of the penalization parameter, η, on the computed solution and the boundary conditions, we perform numerical computations of the shock-cylinder test for different values of η and compute the relative velocity and energy errors inside the obstacle as:

$$\|(u,v)\|_{L_2(\Omega_s)} = \frac{1}{M_{\mathbf{v}}} \left(\delta x \delta y \sum_{(x_i,y_j) \in \overline{\Omega}_s} \|(u,v)_{ij}\|^2 \right)^{1/2}, \qquad (26)$$

$$\|E - E_{\Omega_s}\|_{L_2(\Omega_s)} = \frac{1}{M_E} \left(\delta x \delta y \sum_{(x_i,y_j) \in \overline{\Omega}_s} |E_{ij} - E_{\Omega_s}|^2 \right)^{1/2}, \qquad (27)$$

with $M_{\mathbf{v}} = \max\{\|(u,v)_{ij}\|, (x_i,y_j) \in \Omega\}$ and $M_E = \max\{|E_{ij}|, (x_i,y_j) \in \Omega\}$. The values of $\|(u,v)\|_{L_2(\Omega_s)}$ and $\|E - E_{\Omega_s}\|_{L_2(\Omega_s)}$ obtained from the simulations corresponding to values of η between 10^{-4} and 10^{-10} are plotted in figure 2.

It is interesting to mention that the theoretical estimates for incompressible flows obtained in [2], provide a convergence rate inside the solid obstacle of order $O(\eta^{3/4})$, but the effective, computational, rate inside the solid body in numerical simulations was of $O(\eta)$, a fact that was further confirmed in subsequent papers [16,17,26,31,34]. Our penalization technique seems to follow the same track, since in figure 2, we clearly observe that $\|(u,v)\|_{L_2(\Omega_s)}$ and $\|E - E_{\Omega_s}\|_{L_2(\Omega_s)}$ also tend to zero as $O(\eta)$.
This numerical study indicates that, for practical simulations, the user dependent parameter η allows for a real control of the boundary conditions. In all the remaining simulations of this paper, we set the value $\eta = 10^{-12}$.
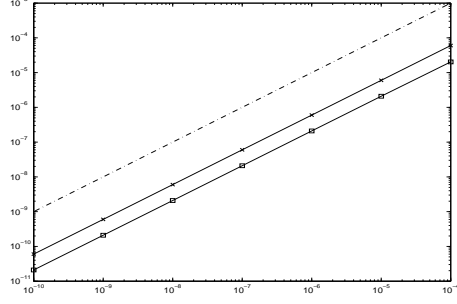
14

Fig. 2. Relative velocity (cross) (26), and energy (square) (27) norms inside the cylinder with respect to the penalization parameter η (dot lines: $f(\eta) = 10 \cdot \eta$, logarithmic scales).

For this value of η, a Schlieren plot of the density after the interaction has taken place is displayed on figure 1(right). Upstream of the obstacle, we clearly observe a well resolved reflected (detached) shock wave, while a more complex structure is developing downstream.

In figure 3 we display 1D profiles of the different flow variables at the two lines crossing the center of the cylinder, whose boundaries are depicted by vertical lines in the plots. The plots corresponding to the velocity norm, computed as $\|(u,v)_{ij}\| = (u_{ij}^2 + v_{ij}^2)^{1/2}$, along the lines $y = 1$ and $x = 0.5$ allow us to see that the velocity field becomes zero at the boundary of the obstacle (its value is in fact of the order of η, see [7]). Likewise, the temperature is equal to the prescribed value of $T_{\Omega_s} = 3$ at the obstacle boundary (up to $O(\eta)$), and remains constant inside the obstacle. Pressure and energy are nearly constants while the density increases rapidly in front of the solid to return to its initial value inside the solid body. This effect is due to the rapid decrease in temperature, and can be explained by the perfect gas law where the density is proportional to $\frac{P}{T}$.

Notice that the values inside of the solid domain remain nearly constant, even though they are not relevant from a physical point of view. This feature implies in turn that, due to the multi-level computation of the numerical divergence, no costly HRSC computations are being made inside the obstacle.

5.2 Steady-state supersonic flow around a triangle

We consider next the flow field over a solid body moving at supersonic speeds. In this section we consider a solid body of triangular shape with height $h = 0.5$ and half angle $\theta = 20 \deg$, as shown in figure 4, placed in the computational domain Ω so that its left apex is located at the point $S = (0.5, 1)$. The flow field is solved using the penalized Navier-Stokes equations (9). The computation is stopped when a steady state is obtain for the position of the shock waves. Once the inlet flow Mach number M_1 is given, the initial variables in the fluid
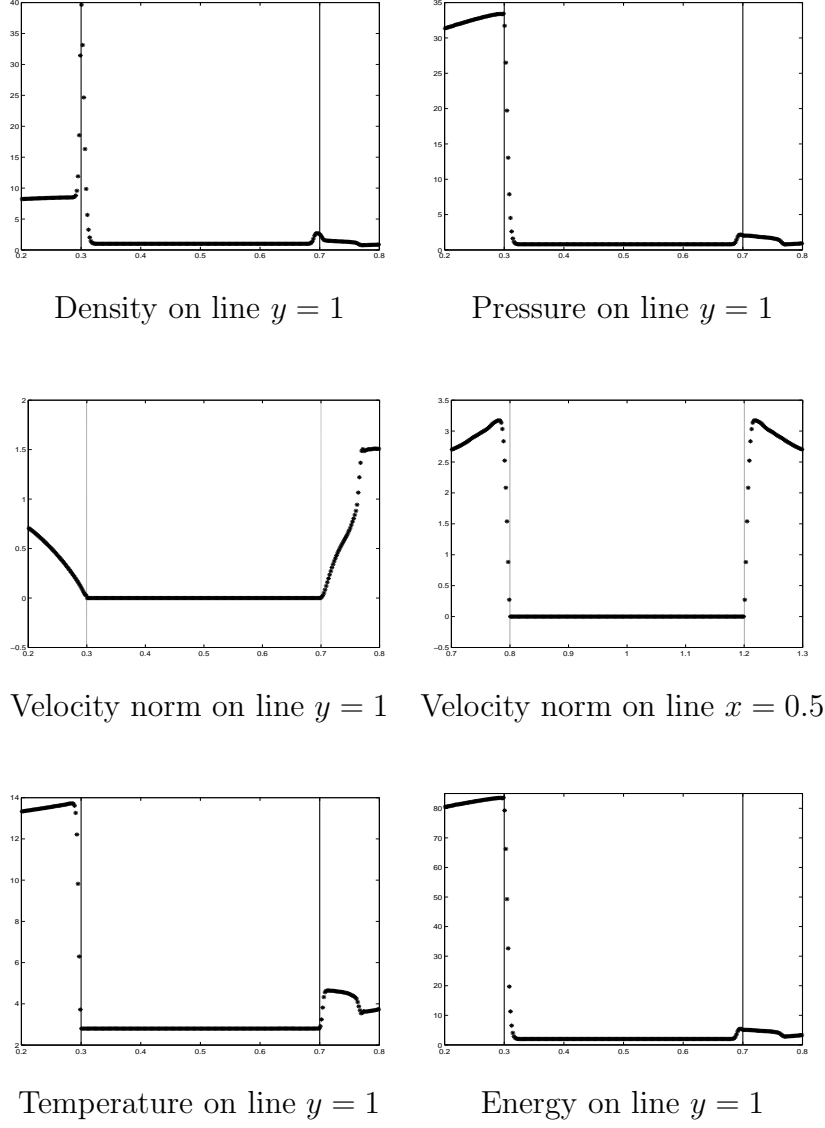
Density on line $y = 1$

Pressure on line $y = 1$

Velocity norm on line $y = 1$

Velocity norm on line $x = 0.5$

Temperature on line $y = 1$

Energy on line $y = 1$

Fig. 3. Profiles of the density, pressure, velocity norm, temperature and energy for the shock-cylinder interaction ($M_s = 3$ and $\eta = 10^{-12}$) along the stagnation line $y = 1$ and along the vertical line $x = 0.5$. The vertical lines define the limits of the solid body.
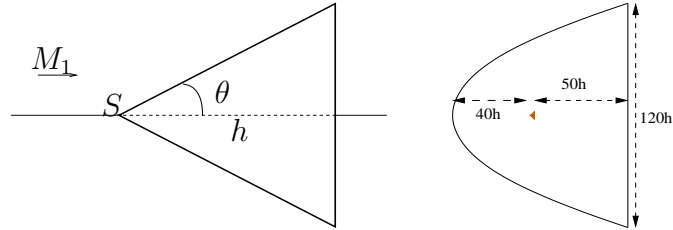

Fig. 4. Left: geometrical configuration for oblique shock wave analysis. Right: Computational domain with Fluent expressed by a multiple of h, the characteristic length of the obstacle.

16

domain, $(\rho_1, p_1, u_1, v_1) = (1, 1, \sqrt{\gamma} M_1, 0)$, are forced at the inlet boundary $x = 0$ for all time. In the solid body we set $\rho = 1$, $T_{\Omega_s} = 3$ and the velocity is set to zero.

A oblique shock is predicted by the inviscid flow theory. It can be attached or detached depending on the values of the deflection angle θ and the upstream Mach number M_1. If the shock is attached to the triangle, its angle with the horizontal, β, can be computed through the following relation [15]:

$$\tan \theta = 2 \cot \beta \left[\frac{M_1^2 \sin^2 \beta - 1}{M_1^2 (\gamma + \cos 2\beta) + 2} \right]. \tag{28}$$

For $M_1 = 2$ and $\theta = 20 \deg$, the shock must be attached and according to (28), $\beta = 53.46 \deg$.
Figure 5 shows Schlieren plots of the density and isomach lines obtained with the penalization technique. The simulation gives an attached oblique shock wave as predicted by the theory.
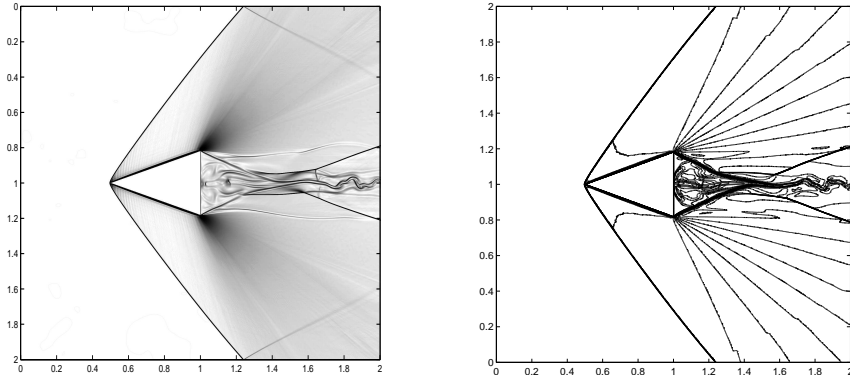Following the Fluent user's guide [11], a larger computational domain is con-

Fig. 5. Supersonic flow around a triangle for $M_1 = 2$ (1536^2 grid points) - Numerical Schlieren image obtained from the density (left) and Isomach lines (right).

sidered in order to minimize the effect of the far field boundary conditions (see fig (4)). A non reflective pressure far field boundary condition is used in order to model a free stream condition on the top boundary, at the bottom boundary and on the left (*i.e.* in the upstream direction) of the solid body. Downstream, a standard pressure boundary condition is set, with a non reflecting treatment of the pressure waves [11]. The boundary conditions on the solid obstacle are $(u, v)_{|\Gamma_s} = (0, 0); T_{|\Gamma_s} = 3$. The adaptive unstructured grid was initially made of 35000 triangular cells and reached 50000 cells during the computation. It corresponds to a spatial resolution around obstacle and shock waves in-between the 512^2 and 1024^2 penalization simulations. The isomach lines of the flow pattern obtained after using the Fluent package are displayed in figure 6. Only part of the computational domain is represented on figure 6.

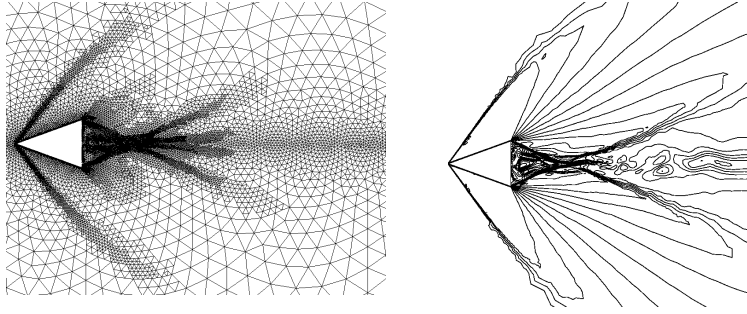From the numerical results, we measure the mean value of the shock angle

Fig. 6. Left: zoom of the computational mesh for the Fluent solver. Right: Isomach lines

for the different computational mesh sizes used in the multilevel-penalization simulations and in the Fluent simulation. For the simulations with the penalization technique (figure 5), we use the left apex of the triangle and the intersection of the shock wave with the $y = 0$ line. The same corresponding points have been used for the Fluent evaluation. The results are displayed in Table 1, where we observed an excellent agreement between numerical and theoretical values.

Theoretical	512^2 grid pts	1024^2 grid pts	1536^2 grid pts	Fluent
$\beta = 53.46\,\mathrm{deg}$	54.13	53.70	53.56	53.62

Table 1
Theoretical and numerical values of mean shock angle β for $M_1 = 2$ and $\theta = 20\,\mathrm{deg}$

Another quantity that can be directly computed from oblique-shock theory for inviscid flow is the value of the pressure downstream of the shock, p_2. It is given by the relation [15]:

$$\frac{p_2}{p_1} = 1 + \frac{2\gamma}{\gamma + 1}\Big((M_1 \sin \beta)^2 - 1\Big). \tag{29}$$

On figure 7, we display the values of the pressure as a function of x on the line $y = 1.44$, a line located sufficiently far from the solid body so that it is reasonable to assume that the flow is inviscid there. We readily appreciate the good agreement between the results obtained by the penalization technique and the Fluent results.

In addition, we compile in table 2 the various numerical estimates for the value of p_2 obtained from the numerical values in the above plots, together with the theoretical value predicted by (29). The results obtained with the penalization technique are a mere .5% off the values predicted by the inviscid flow theory.

For high Mach number flows, like in the present situation, the viscous drag is less than 2% of the total drag exerted on the body. Indeed, even if the grid resolution is not sufficient to fully resolve the viscous layer around the solid
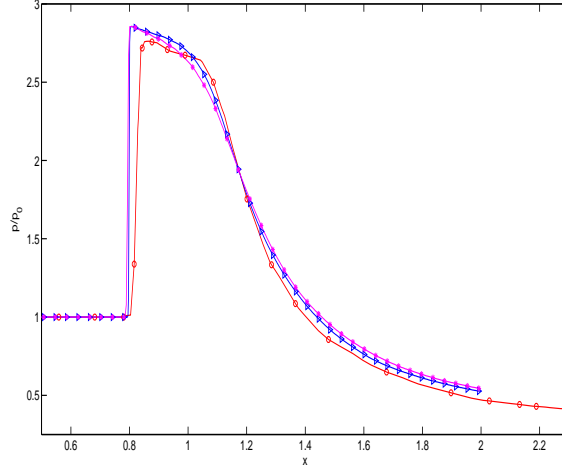
Fig. 7. Supersonic flow around a triangle for $M_1 = 2$ - Pressure on line $y = 1.44$. Fluent simulation ($\circ$); penalization with 1024^2 points ($\triangleright$) and with 512^2 points ($\star$).

Theoretical	512^2 grid pts	1024^2 grid pts	1536^2 grid pts	Fluent
$p_2 = 2.8458$	2.859	2.86	2.864	2.759

Table 2
Theoretical and numerical values of p_2 at point A of coordinates $(0.8, 1.44)$.

body, computation of the drag is physically relevant. The total drag coefficient, C_D^T, is computed as usual dividing the x-component of the force acting on the solid by the quantity $\frac{1}{2}\rho_1 u_1^2 l$, where l is the length of the body (the height of the triangle in our case). For the flow computation we carried out in this section, (and with our dimensionless variables) $l = .5$, $M = 2$ so that the formula reduces to $C_D^T = \mathbf{F}_{\Omega_s}^x / \gamma$. The Fluent package provides directly the value of C_D^T, while in the penalization simulations, we can estimate its value using formula (17) and simple numerical integration:

$$\mathbf{F}_{\Omega_s}^x \approx \frac{\delta x \delta y}{\eta} \sum_{(x_i, y_j) \in \Omega_s} \rho(x_i, y_j) \, u_\eta(x_i, y_j). \tag{30}$$

It is also possible to deduce an approximate value of the pressure drag coefficient, C_D^P, using classical inviscid shock wave and Prandtl-Meyer theories [32]. The derivation assumes a constant static pressure on the back side of the body, p_3, equal to the downstream expansion wave pressure value, giving rise to:

$$C_D^P = \frac{4(\frac{p_2}{p_1} - \frac{p_3}{p_1}) \tan \theta}{\gamma M_1^2}. \tag{31}$$

From the Fluent results, we measure a value of $p_3 = 0.22$ after the expansion wave, which, substituting in (31) gives $C_D^P \approx 0.68$. The Fluent package provides directly a value for C_D^P (see table 3), which is very close to this approximation but also to C_D^T, as it should be for this flow. The results for the

19

	Penalization	Fluent	Euler theory
C_D^T	0.743/0.717/0.727	0.709	#
C_D^P	#	0.704	0.68

Table 3
Total and Pressure Drag coefficients for Mach 2 inlet flow on a triangle. Penalization results are for $512^2/1024^2/1536^2$ grid points.

flow under examination are displayed in table 3, were we can observe the excellent agreement between the values obtained by the two techniques.

We conclude this section by emphasizing the robustness of the multilevel penalization technique for high Mach number flows. In figure 8, we present the numerical results obtained with this technique for a Mach 4.9 flow. In this case, formula (28) yields a theoretical angle $\beta = 30.0058$ deg, and relation (29) gives a value for the downstream pressure of $p_2 = 6.8387$. We measure these quantities from our numerical results, obtaining an numerical estimate for the reflected shock of $\tilde{\beta} = 29.92$ deg using the left apex and the intersection of the shock and the $x = 2$ line. An estimate for p_2 is obtained by the numerical value for the pressure at the point $(1.3, 1.5)$, this value yields $\tilde{p}_2 = 6.745$. These encouraging results give an indication of the robustness of the numerical technique, HRSC plus penalization, even for high Mach number flow.
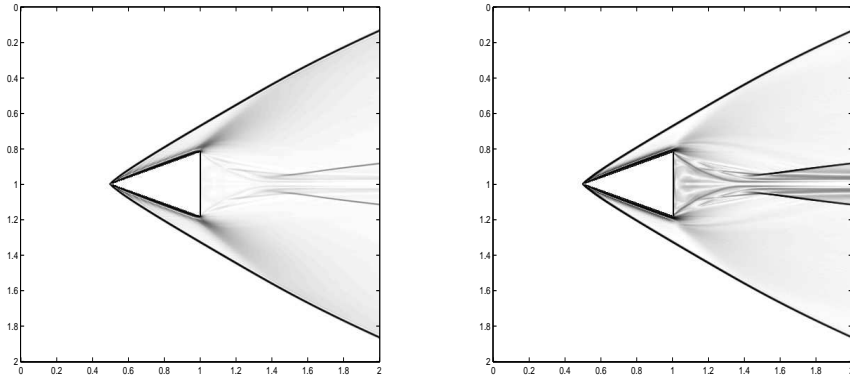

Fig. 8. Supersonic flow around a triangle for $M_1 = 4.9$ (512^2 grid points) - Numerical Schlieren image obtained from the density (left) and the temperature (right).

5.3 Steady-state supersonic flow around a cylinder

It is well known that a blunt-nosed body moving at supersonic speeds produces a strong, curved bow shock wave which sits in front of the blunt-nose. In the case of a solid cylinder, some properties of the flow, like the geometrical form of the shock, or its position behind the cylinder, have been studied in inviscid flow

theory. We shall use them to further validate the numerical results obtained with our penalization technique.

We consider a cylinder of radius $r = 0.2$, centered at the point $(1, 1)$ in our usual computational domain Ω. The initial and inflow values of density, pressure and velocity are as in section 5.2 and the same no-slip and temperature boundary conditions are applied on the obstacle. Numerical solutions obtained for $M_1 = 2$ are represented on figure 9.
From theoretical and experimental results, Billig proposed in [4] to model the geometrical form of the shock wave by a hyperbola. Then, the distance Δ of the shock from the obstacle, measured on the stagnation line ($y = 1$), is approximated in [4] by:

$$\frac{\Delta}{r} = 0.386 \exp\left(\frac{4.67}{M_1^2}\right). \tag{32}$$

We have superposed Billig's hyperbola to the results of our simulations in figure 9. It can be observed that there is a very good agreement in the region surrounding the stagnation line $y = 1$. This is further confirmed by the numerical estimates of Δ obtained from our simulations, which are displayed in Table 4, where the results obtained from the Fluent simulation are also provided. The same computational domain and boundary conditions than in section 5.2 are used for the Fluent simulation and isodensity lines are provided on fig 9. In fig 9, it should also be noticed the discrepancy between the theoretical and computational shapes of the bow shock near the upper and lower boundaries of the domain Ω. This behavior can be blamed on the imposed outflow condition on these boundaries, which perturbs the flow and slows down the shock wave, and we have verified that the computation on a slightly wider domain decreases the difference at boundaries. This drawback could be avoided using a more sophisticated treatment of these outflow boundaries, but this is out of the scope of this paper at this moment.

$M_1 = 2$	Theoretical	Penalization	Fluent
Δ/r	1.24	1.33/1.23	1.30
p_s	5.69	5.65/5.68	5.608

Table 4
Theoretical and numerical values of shock detachment Δ/r and stagnation pressure for Mach 2 flow-cylinder interaction. Numerical values are given for $512^2/1024^2$ grid points.

The accuracy of the computed flow close to the stagnation line is further examined as follows. In figure 10, we display the value of the pressure along the stagnation line $y = 1$ for two values of the mesh size in the penalization simulations, together with the Fluent results. There is an excellent agreement between these sets of numerical values.
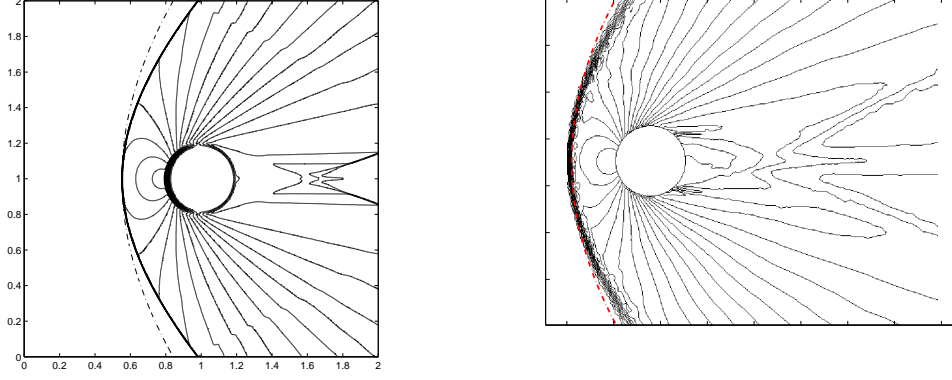
Fig. 9. Supersonic flow around a cylinder for inlet Mach number $M_1 = 2$. Left: isodensity lines computed with penalization method and 1024^2 grid points. Right: isodensity lines computed with Fluent. Dotted lines: Billig's hyperbola approximation of bow shock.
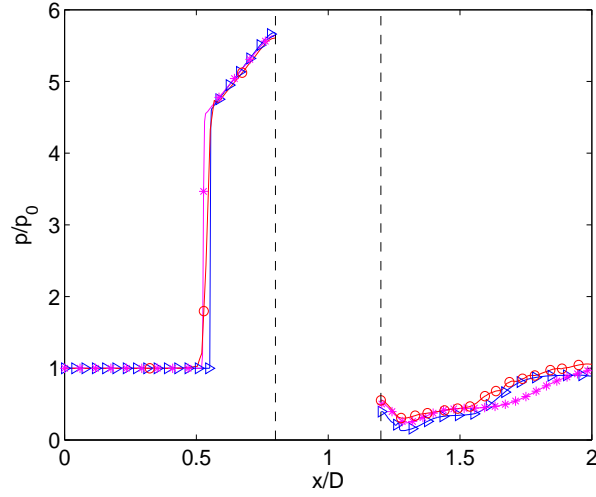

Fig. 10. Supersonic flow around a cylinder for $M_1 = 2$ - Pressure on line $y = 0$ - Fluent simulation ($\circ$); penalization with 1024^2 points ($\triangleright$) and with 512^2 points ($\star$).

In addition, we shall also compare the value of the stagnation pressure $i.e$ $p(0.8, 1)$, to the theoretical value provided by compressible flow theory [15]. The value of p_s is given as a function of p_l and M_l, the values of pressure and Mach number on the stagnation line ($y = 1$) just after the bow shock, by the following relation:

$$p_s = p_l(1 + \frac{\gamma - 1}{2}M_l^2)^{\frac{\gamma}{\gamma-1}}. \tag{33}$$

We measure p_l and M_l from our simulations to obtain the prediction of p_s by formula (33). In table 4, we compare this value to the pressure given by our code at the stagnation point, ($x = 0.8, y = 1$). The very good agreement obtained, confirms the ability of our method to compute precisely important physical parameters in flow-obstacle interactions.

22

	Penalization	Fluent
C_D^T	1.43/1.44	1.358
C_D^P	#	1.357

Table 5
Total and Pressure Drag coefficients for Mach 2 inlet flow on a cylinder. Penalization results are for $512^2/1024^2$ grid points.

In table 5, we display the drag coefficients computed from our numerical results. For the penalization method we use $l = .4$, i.e. the diameter of the cylinder and, following the same arguments as before, we arrive at the formula $C_D^T = 5\mathbf{F}_{\Omega_s}^x/(4\gamma)$. There is only a .5% discrepancy between the results obtained with both techniques.

We close this section with a final simulation that emphasizes the ability of the penalization technique to deal with complex geometrical configurations. In figure 11, we show the results of the simulation of the interaction of a Mach 3 shock wave with six cylinders. The initial set-up is the same as in section 5.1. This configuration would be difficult to manage for any classical method, increasing, in many cases, the computational expense with respect to that of a single cylinder. However, the penalization algorithm we have introduced in this paper only needs the characteristic function of the solid bodies. Absolutely no extra cost is added compared to the one-obstacle computation of section 5.1, except from the fact that the multiple shock interactions produce a rather complex flow pattern, detected by the multilevel technique, so that a larger number of costly flux evaluation is demanded by the flow field. However,this is an automatic feature of the multilevel procedure and the basic code is exactly the same. Only the mask function needs to be modified to account for the six cylinders.

6   Conclusion

In this paper, we have performed a series of numerical experiments that aim at evaluating a new penalization technique, proposed in [7], for compressible flow in the presence of solid obstacles. The proposed penalization technique was motivated by the Brinkman-penalization technique analyzed in [2] for incompressible flows, and it involves the addition of penalization terms in the momentum and energy equations of the 2D compressible Navier-Stokes system. A formal perturbation analysis, confirmed by our numerical experiments, shows that the proposed penalization effectively imposes no-slip boundary conditions on the velocity and Dirichlet boundary conditions on the temperature of the obstacle.
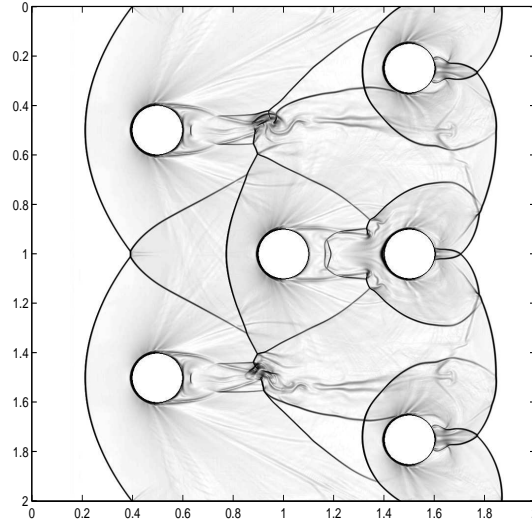The main purpose of penalization techniques is to avoid the use of body fitted

Fig. 11. Multi-cylinders simulation with an initial Mach 3 shock wave (Density 1024^2 grid points at time $t = 0.5$).

meshes in order to be able to use fast and effective methods on Cartesian grids. In order to solve the penalized equations, we follow the multilevel strategy of [6], which is based on a method-of lines discretization of the penalized system on a regular Cartesian mesh. The resulting system of ODEs are solved in time by a TVD Runge-Kutta scheme with an implicit treatment of the penalization terms. The specific form of the penalization terms in our method results in a diagonal system whose solution does not involve any additional cost. The high resolution shock capturing technology is used for the explicit discretization of the convective fluxes, and we use a simple explicit treatment of the viscous, second order, terms in the equations.

The explicit treatment of the parabolic terms is justified by the fact that we aim at simulations at large Reynolds number, and the high resolution shock capturing technology is essential in order to obtain reliable results for high Mach number flows. The multi-level cost reduction strategy allows for a significant reduction of the computational cost associated to the numerical flux computations, [6,28] and allows us to obtain high resolution simulations at reasonable computational times on personal computers (between hour and day for the presented simulations).

The numerical results shown in this paper suggest that the convergence rate to the right no-slip and temperature conditions inside the obstacle is proportional to the penalization parameter η, the same computational rate observed in the incompressible case. Since η is an independent parameter, this implies a real control on the way the boundary conditions are imposed.

Several numerical simulations involving high Mach numbers flows and solid bodies of different shapes have been presented. The results have been compared to well-known properties of inviscid shocked flows, and also with the Fluent package for CFD computations. The numerical results presented show

24

the ability of our method to represent precisely and efficiently important properties of the flow away from the boundary of the obstacle. In this paper, only Euler-like behavior has been analyzed.

More mathematical aspects of this method need also to be analyzed, including the convergence of the penalized solution to the solution of the original problem in the flow domain region.
From the computational point of view, it will be interesting to examine the improvements that result from considering a higher accuracy in the implicit treatment of the penalization terms, as well as to consider simulations on aerodynamic bodies, such as airfoils, which will also contribute to better understand and evaluate the potential of the proposed technique. It is important also to study the behavior of the solution close to the solid body, and in all regions where the viscous effects are important.

Another important issue that has not been considered in this paper is that of the accuracy of the results obtained. For this, a numerical study with respect to known exact solutions is needed. This will be considered in a forthcoming paper.

Nevertheless, these first difficult simulations point out that our penalization method, combined with a robust HRSC technique, could be efficiently used in the future in numerical simulations involving complex industrial flows.

Acknowledgments

References

[1] J.D. Anderson Jr., *Modern Compressible Flow* , Series in Mechanical Engineering, McGraw-Hill, (1982).

[2] P. Angot, C.-H. Bruneau and P. Fabrie, *A penalization method to take into account obstacles in incompressible flows*, Numer. Math. (1999)81, pp 497-520.

[3] E. Arquis, J.P.Caltagirone, *Sur les conditions hydrodynamiques au voisinage d'une interface milieu fluide-milieu poreux: application à la convection naturelle*, C.R. Acad. Sci. Paris II, 299 (1984), pp 1-4.

[4] F.S. Billig, *Shock-wave shapes around spherical -and cylindrical- nosed bodies*, J. Spacecraft 4(6), (1967).

[5] Y.Cho, S. Boluriaan and P.J. Morris, *Immersed Boundary Method for Viscous Flow Around Moving Bodies*, 44th AIAA Aerospace Sciences Meeting and Exhibit, Nevada, January 2006.

[6] G. Chiavassa, R. Donat, *Point Value Multiscale Algorithms for 2d Compressible Flows*, SIAM J. Sci. Comput., Vol 23-3 (2001), pp 805-823.

[7] G. Chiavassa, R. Donat, *A Penalization technique for the efficient computation of compressible fluid flow with obstacles* , Prooceedings of the XI Intl. Conf. on Hyperbolic Problems: Theory, Numerics, Applications. Ed: S. Benzoni-Gavage, D. Serre. (2007) Springer.

[8] A.Cohen, S.Müller, M.Postel, S.M.Ould-Kaber, *Fully adaptive multiresolution schemes for conservation laws*, Math. Comp. 72,(2002) pp. 183-225.

[9] P. Colella, D.T.Graves, B.J. Keen, D. Modiano, *A Cartesian grid embedded boundary method for hyperbolic conservation laws* J. Comput. Phys. 211 (2006) pp 347-366.

[10] R. Donat, A. Marquina, *Capturing Shock Reflections: An improved Flux Formula*, J. Comput. Phys., 125 (1996), pp 42-58.

[11] *Fluent Users's guide*, vol. 3, (2006) Fluent Inc.

[12] H. Forrer, R. Jeltsch, *A higher-order boundary treatment for Cartesian-Grid Methods* J. Comput. Phys. 140 (1998), pp 259-277.

[13] R. Glowinski, T.W. Pan, R.O. Wells Jr, X. Zhou, *Wavelet and Finite Element Solutions for the Neumann Problem using Fictitious Domains*, J. Comput. Phys., 126(1), pp 40-51 (1996).

[14] A. Harten *Multiresolution Algorithms for the numerical solution of hyperbolic conservation laws*, Comm. Pure Appl. Math., 48 (1995) pp. 1305-1342.

[15] C. Hirsch, *Numerical Computation of Internal and External flows*, I-Fundamental of Numerical Discretization and II- Computational Methods for Inviscid and Viscous Flows, Wiley Series.

[16] N.K.R. Kevlahan, J.M.Ghidaglia, *Computation of turbulent flow past an array of cylinders using a spectral method with Brinkmann penalization*, Eur. J. Mech./B, 20 (2001), pp 333-350.

[17] N.K.R Kevlahan, O.V. Vasilyev, *An Adaptive Wavelet collocation Method for Fluid-Structure Interaction at High Reynolds Number*, SIAM J. Sci. Compt., Vol 26, No 6, (2005).

[18] K. Khadra, S. Parneix, P. Angot, J.P. Caltagirone, *Fictitious domain approach for numerical modelling of Navier-Stokes equations*, Int. J. Num. Mth. Fluids, 34 (2000), pp 651-684.

[19] A. Kunoth, *Wavelet Techniques for the Fictitious Domain-Lagrange Multiplier Approach*, Numer. Algor. 27 (2001) pp 291-316.

[20] R. LeVeque, *Finite Volume Methods for Hyperbolic Problems*, Cambridge Texts in Applied Mathematics, Cambridge University Press, (2002) pp 130-132

[21] R. LeVeque, , D. Calhoun, *A Cartesian Grid Finite-Volume Method for the Advection-Diffusion Equation in Irregular Geometries* J. Comp. Phys., 157 (2000) pp 143-180

[22] C. Helzel, M. Berger, R. LeVeque, *A high-resolution rotated grid method for conservation laws with embedded geometries* SIAM J. Sci. Comput. 26 (2005) pp 785-809.

[23] Q. Liu, O. Vasilyev, *A Brinkman penalization method for compressible flow in complex geometries* J. Comp. Phys., 227 (2007) 946-966

[24] A. Marquina, *Local Piecewise Hyperbolic Reconstruction of Numercial Fluxes for Nonlinear Scalar Conservation Laws*, SIAM J. Sci. Comput., 15 (1994).

[25] S. Müller, Y. Stiriba, *Fully adaptive multiscale schemes for conservation laws employing locally varying time stepping* J. Sci. Comput. 30 (2007) pp. 493-531.

[26] A. Paccou, G. Chiavassa, J. Liandrat, K. Schneider, *A penalization method applied to the wave equation*, C. R. Acad. Sci. Paris, 329 (2003).

[27] J. J. Quirk *An alternative to unstructured grids for computing gas dynamics flows around arbitrarily complex two-dimensional bodies* Computers & Fluids, 23 (1994) pp 125-142.

[28] A. Rault, G. Chiavassa, R. Donat, *Shock-Vortex Interaction at High Mach Numbers*, J. Sci Comput., 19, 1-3(2003), pp 347-372.

[29] O. Roussel, K. Schneider, *An adaptive multiresolution method for combustion problems: application to flame ball-vortex interaction* Comp. Fluids 34, (2005) pp. 817-831.

[30] C.W. Shu, S.J. Osher, *Efficient Implementation of Essentially Non-Oscillatory Shock Capturing Schemes II*, J. Comput. Phys., 83 (1989), pp. 32-78.

[31] K. Schneider, M. Farge, *Adaptive wavelet simulation of a flow around an impulsively started cylinder using penalization*, Appl. Comput. Harm., 12 (2002), pp 374-380.

[32] A.H. Shapiro *Compressible Fluid Flow*, Vol. 1& 2, (1953).

[33] E.F. Toro, *Riemann Solvers and Numerical Methods for Fluid Dynamics*, Springer-Verlag (1999).

[34] O.V Vasilyev, N. Kevlahan, *Hybrid wavelet collocation-Brinkman penalization method for complex geometry flows*, Int. J. Num. Meth. Fluids, 40, (2002).

[35] X. Zhong, *Additive Semi-Implicit Runge-Kutta Methods for Computing High-Speed Nonequilibrium Reactive Flows*, J.Comp. Phys., 128 (1996), pp 19-31.